

Formation of a Partially-Screened Inner Acceleration Region in Radio Pulsars: Drifting Subpulses and Thermal X-Ray Emission from Polar Cap Surface

Janusz Gil^{1,2}, George Melikidze^{1,3} & Bing Zhang ²

ABSTRACT

The subpulse drifting phenomenon in pulsar radio emission is considered within the partially screened inner gap model, in which the sub-Goldreich-Julian thermionic flow of iron ions or electrons coexists with the spark-associated electron-positron plasma flow. We derive a simple formula that relates the thermal X-ray luminosity L_x from the spark-heated polar cap and the $\mathbf{E} \times \mathbf{B}$ subpulse periodicity \hat{P}_3 (polar cap carousel time). For PSRs B0943+10 and B1133+16, the only two pulsars for which both \hat{P}_3 and L_x are known observationally, this formula holds well. For a few other pulsars, for which only one quantity is measured observationally, we predict the value of the other quantity and propose relevant observations that can confirm or discard the model. Then we further study the detailed physical conditions that allow such partially screened inner gap to form. By means of the condition $T_c/T_s > 1$ (where T_c is the critical temperature above which the surface delivers a thermal flow to adequately supply the corotation charge density, and T_s is the actual surface temperature), it is found that a partially-screened gap (PSG) can be formed given that the near surface magnetic fields are very strong and curved. We consider both curvature radiation (CR) and resonant inverse Compton scattering (ICS) to produce seed photons for pair production, and find that the former is the main agency to produce gamma-rays to discharge PSG.

Subject headings: pulsars: general — stars: neutron — X-rays: stars

¹Institute of Astronomy, University of Zielona Góra, Lubuska 2, 65-265, Zielona Góra, Poland

²Department of Physics, University of Nevada, Las Vegas, USA

³CPA, Abastumani Astrophysical Observatory, Al. Kazbegi ave. 2a, 0160, Tbilisi, Georgia

1. Introduction

Pulsar radio emission typically occurs in a form of periodic series of narrow bursts of radiation. These bursts often have a complex structure, in which higher order periodicities can be found. The individual pulses consist of one, few to several subpulses. In some pulsars the subpulses demonstrate a very systematic drift across the pulse window. If the pulses are folded with the basic pulsar period then the drifting subpulses form amazingly spectacular patterns called drift-bands.

The phenomenon of drifting subpulses is a long standing puzzle in the pulsar research and its solution would likely result in deeper understanding to the nature of pulsar radiation. It is generally believed that this phenomenon is inherently associated with the so-called inner acceleration region above the polar cap, in which the magnetosphere's plasma does not corotate with the neutron star surface. The first model based on this idea was proposed by Ruderman & Sutherland (1975, RS75 henceforth). The predictions of RS75 model were successfully compared with a handful of pulsars known to show this phenomenon at that time. A decade later, Rankin (1986, R86 hereafter) compiled a list of about 40 drifting pulsars, but drifting subpulses were still regarded as some kind of exceptional phenomenon. However, recently Weltevrede, Edwards, & Stappers (2006, WES06 hereafter) presented the results of a systematic, unbiased search for subpulse modulation in 187 pulsars and found that the fraction of pulsars showing drifting subpulse phenomenon is likely to be larger than 55%. They identified 102 pulsars with drifting subpulses in their sample, with a large fraction of newly discovered drifters. The authors concluded that the conditions required for the drifting mechanism to work cannot be very different from the emission mechanism of radio pulsars. WES06 then suggest that the subpulse drifting phenomenon is an intrinsic property of the pulsar emission mechanism, although drifting could in some cases be very difficult or even impossible to detect due to insufficient signal-to-noise ratio. It is therefore essential to attempt to unravel the physical conditions that can lead to formation of an inner acceleration region above the polar cap that could lead to development of the subpulse drift phenomenon.

The classical vacuum gap model of RS75, in which spark-associated sub-beams of subpulse emission circulate around the magnetic axis due to $\mathbf{E} \times \mathbf{B}$ drift of spark plasma filaments, provides the most natural and plausible explanation of drifting subpulse phenomenon. However, despite its popularity, it suffers from the so-called binding energy problem. Namely, under canonical conditions the surface charges (ions or electrons) are likely to be directly pulled out of the surface so that a pure vacuum gap is difficult to form. The alternative steady flow polar cap models, the so-called space-charge-limited flow models (Arons & Scharlemann 1979; Harding & Muslimov 1998), cannot give rise to the intermittent “spark-

ing” behavior, which seems necessary to explain the subpulse drift phenomenon in radio pulsars. Gil & Mitra (2001, GM01 hereafter) revisited the binding energy problem of RS75 model and argued that the formation of the vacuum gap (VG) is, in principle possible, although it requires a very strong non-dipolar surface magnetic fields, much stronger than a canonical dipolar component inferred from the observed spindown rate. Once the binding is strong enough to prevent the thermionic emission at the full space charge limited flow, the inevitable $\mathbf{E} \times \mathbf{B}$ drift of plasma filaments will result in the observable subpulse drift phenomenon. It has been known for a long time that in order to allow all radio pulsars to produce electron-positron pairs (the necessary condition for coherent radio emission), the near-surface magnetic fields must include multipole components dominating over global dipole field (Ruderman & Sutherland 1975; Arons & Scharlemann 1979; Zhang, Harding, & Muslimov 2000). Growing observational evidence of non-dipolar structure of surface magnetic field ¹ accumulates, and the suggestion that such a sunspot-like fields form during the early proto-neutron star stage has been proposed ² (e.g. Urpin & Gil 2004). Gil & Melikidze (2002, GM02 hereafter) calculated the non-dipolar VG model for 42 drifting subpulse pulsars tabulated by R86 and argued that VG can be formed in all considered pulsars, provided that the actual surface magnetic field was close to 10^{13} G independently of the value of the canonical dipolar magnetic field.

Although the binding energy problem could be, at least in principle, resolved by assuming an appropriately strong surface magnetic field, yet another difficulty of the RS75 model was that it predicted a much too fast $\mathbf{E} \times \mathbf{B}$ drift rate. Motivated by this issue, Gil, Melikidze, & Geppert (2003, GMG03 hereafter) developed further the idea of the inner acceleration region above the polar cap by including the partial screening by a sub-Goldreich-Julian thermal flow from the surface due to the spark-associated polar cap heating. This idea was first introduced by (Cheng & Ruderman 1980, CR80 henceforth), who argued that even with thermionic ions included in the flow, the condition above the polar cap is close to that of a pure vacuum gap. A similar model was also invoked by Usov & Melrose (1995, 1996). GMG03 reanalyzed this model and argued that a thermostatic self-regulation should keep the surface temperature just few percent below the critical ion temperature at which the gap potential drop is completely screened. This results in more than 90 % of screening

¹It is worth mentioning that although RS75 implicitly assumed non-dipolar surface magnetic fields to treat the γ - B pair production processes, in their calculations of many other physical quantities (such as the surface charge density) they still used dipolar form, presumably for the sake of simplicity.

²Another possible mechanism of creating small scale anomalies of surface magnetic fields was proposed by Geppert, Reinhardt & Gil (2003). They argued that due to a Hall drift instability, the poloidal magnetic field structures can be generated from strong subsurface toroidal fields.

due to thermionic emission. Given a similar gap height, the actual potential drop, and hence the $\mathbf{E} \times \mathbf{B}$ drift rate, is about 10 % of that of the pure vacuum case. This is still above the threshold for the magnetic pair production. Similar to the avalanche pair production cascade introduced by RS75, the discharge of the growing potential drop above the polar cap would also occur in the form of a number of sparks. In this paper we call such an inner accelerator a partially screened gap (PSG henceforth). The latest XMM-Newton observation of the drifting pulsar PSR B0943+10 (Zhang, Sanwal, & Pavlov 2005, ZSP05 hereafter) reveals a possible hot spot with the surface area much smaller than the conventional polar cap. This is consistent with the polar cap heating from such a PSG, which at the same time gives the right $\mathbf{E} \times \mathbf{B}$ drift rate. This lends strong support to the PSG model.

In this paper we study PSG model in greater detail and explore the physical conditions for the model to work. We also apply this model to a new set of 102 pulsars from WES05 and show that it can work in every case, provided that the surface non-dipolar magnetic field is strong enough, even stronger than 10^{13} G suggested by GM02 and GMG03. Our new treatment is a combination of those used in GM02 and GMG03. Our working hypothesis is that drifting subpulses manifest the existence of a thin inner acceleration region, with an acceleration length scale much shorter than the polar cap size. The ultra-high accelerating potential drop discharges via a number of localized $\mathbf{E} \times \mathbf{B}$ drifting sparks, as has been envisioned by RS75. These sparks produce isolated columns of electron-positron plasma that stream into the magnetosphere to generate radio-beams of the observed subpulse emission due to some kind of plasma instability (see the §8 for more discussion). Due to charge depletion with respect to the co-rotational Goldreich-Julian (1969) value, sparks experience an unavoidable $\mathbf{E} \times \mathbf{B}$ drift with respect to the polar cap surface. As a consequence, the spark-associated sub-beams of radio emission perform a slow circumferential motion that is responsible for the observed subpulse drift. This model, which is often called “a pulsar carousel model” (Deshpande & Rankin 1999), is examined in this paper³. We are particularly interested in the thermal effect associated with the surface bombardment by back-flowing particles produced by sparks. The intrinsic drift rate (manifested by the tertiary drift periodicity) and the polar cap heating rate (manifested by the thermal X-ray luminosity) should be correlated with each other, since they are determined by the same value of the accelerating potential drop. The properties of drifting subpulses are discussed in §2 and the properties of charge depleted acceleration region above the polar cap are discussed §3. We

³Other suggestions of subpulse drifting as phenomena occurring outside the inner gap have been made (Kazbegi, Machabeli & Melikidze 1991; Spitkovsky & Arons 2002; Wright 2003; Gogoberidze, Machabeli, Melrose, et al. 2005; Fung, Khechinashvili & Kuijpers 2006), but the connection between the radio drifting rate and the X-ray properties in those models is not yet clear, and we do not discuss them in the current paper.

find a specific relationship between the appropriate observables and conclud that it holds for a number of pulsars for which good quality data is available (especially PSR B0943+10, ZSP05). It turns out that this relationship depends only on the observational quantities and thus it is a powerful tool for testing this theoretical model. Although the number of pulsars that have all necessary data for such testing is small at the moment, the clean prediction holds the promise to ultimately confirm (or discard) the PSG model in the future. In §§4-7 we analyze this model in a more detailed manner to investigate the microscopic conditions (e.g. near-surface configuration, radiation mechanism, etc) that are needed to form such PSGs. The paper is summarized in §8.

2. Drifting subpulse phenomenon

Let us briefly review the characteristic properties of the drifting subpulse phenomenon, in which subpulses typically change phase from one pulse to another in a very organized manner, to the extent that they form apparent driftbands of duration from several to a few tens of consecutive pulses. Usually more than one drift band appears, and the separation between them measured in pulsar periods ranges from about 1 to about 15 (Backer 1976; Rankin 1986). The subpulse intensity is systematically modulated along drift bands, decreasing towards the edges of the pulse window. In some pulsars, however, only periodic intensity modulations are observed, without any systematic phase change. These pulsars were identified as those in which the line-of-sight cuts through a beam centrally (Backer 1976), thus showing a steep gradient of the polarization angle curve (e.g. Lyne & Manchester 1988). On the other hand, the clear subpulse driftbands are typically found in pulsars associated with the line-of-sight grazing the beam, thus showing a relatively flat position angle curve (Backer 1976; Rankin 1986; Lyne & Manchester 1988). It is then obvious that both these kinds of subpulse behavior, i.e. systematic drift in phase and phase stationary intensity modulation, represent the same phenomenon, namely, rotation of beams of subpulse emission around the pulsar magnetic axis. The picture of rotating subbeams is also supported by spectral properties of the observed radiation. The separation between drifting subpulses in a given pulse show dependence on frequency similar to those of profile components and/or overall pulse width, while the observed periodicities related to patterns of drifting subpulses are independent of radio frequency. This seems to exclude all frequency-dependent plasma effects as a plausible source of the drifting subpulse phenomena. Also, a similarity of drift patterns at different radio frequencies strongly suggest that the radiation of drifting subpulses is related to a relatively stable system of isolated plasma filaments originating near the polar cap.

The observational characteristics of drifting subpulses described briefly above suggest

then strongly an interpretation of this phenomenon as a number of isolated sub-beams of radio emission, spaced more or less uniformly in the magnetic azimuth, and rotating slowly around the magnetic axis. In terms of RS75 model this means that the subpulse-associated sparks perform a circumferential motion around the pulsar beam axis. The most spectacular confirmation of this "carousel model" was presented by Deshpande & Rankin (1999, 2001) and Asgekar & Deshpande (2005), who performed a sophisticated fluctuation spectra analysis of single pulse data from PSR B0943+10 and detected clear spectral features corresponding to the rotational behavior of subpulse beams. These results indicate clearly that sparks do not vanish after passing through the pulse window in the form of drifting subpulses, but they continue to drift around the polar cap and reappear in the same phase of the pulse window after a definite and measurable time period. The rotational features appearing in the fluctuation spectra of PSR B0943+10 have extremely high values of $Q \sim 500$ (defined as the central frequency divided by the width) confirming a circulatory nature of the phenomenon. Similar feature with $Q \sim 100$ was found by Asgekar & Deshpande (2005) in PSR B0834+06. Quite recently Gupta, Gil, Kijak, et al. (2004) revealed a system of subpulse beams circulating around the polar cap in PSR B0826-34. The high values of Q suggests strongly that the trajectories of the spark motion associated with drifting subpulses should be closed. It is natural to conclude that the circulating sparks would form on average in a ring on the polar cap corresponding to a conal beam of radio emission originating at some height above the polar cap (Gil, Kijak & Seiradakis 1993; Kijak, & Gil 1998).

The "pulsar carousel model" based on $\mathbf{E} \times \mathbf{B}$ drifting sparks is widely accepted by radio-observers but theorists usually treat it with a great deal of reservation. Besides the binding energy problem (see §4), they usually point out problems with spark stability and memory, which is indeed necessary to explain the systematic subpulse drift within the carousel model. This is a very important but difficult problem that requires sophisticated computer simulations. Here we would only raise some phenomenological arguments. Following RS75, Gil & Sendyk (2000; GS00 henceforth) argued that both the characteristic spark dimension and the typical distance between the adjacent sparks are approximately equal to the gap height. At any instant the polar cap should be populated by as many sparks as possible. Indeed, spark discharges should develop wherever the accelerating potential drop exceeds the threshold for the magnetic pair production. Such a maximum packing should stabilize an instantaneous arrangement of sparks on the polar cap surface. Each spark develops and dies over a time scale of microseconds, so the question is what agency makes them to reappear in the same place (such reappearance is necessary to explain the regular subpulse drifting). It seems that a natural reason is thermal emission of charges at the base of each spark is heated by the return bombardment. Moreover, some electrons and positrons from the outflowing spark plasma column would still be near the polar cap surface when the returning potential

drop again exceeds the pair formation threshold. These charged particles would initiate the very next discharge (see Asseo & Melikidze 1998; Melikidze, Gil & Pataraya 2000, and GS00 for more detailed discussion). Therefore, the only net motion of sparks is the slow $\mathbf{E} \times \mathbf{B}$ drift across the planes of the surface magnetic field. For the line-of-sight grazing the pulsar beam (corresponding to sparks operating at the polar cap boundary), this circumferential drift motion will be observed as a systematic subpulse drift, while for a more central line-of-sight trajectories only longitude-stationary modulation of the subpulse amplitude can be observed.

3. Charge depleted inner acceleration region

The inner acceleration region above the polar cap may be a result of deviation of the local charge density ρ from the co-rotational charge density (Goldreich & Julian 1969, GJ69 hereafter)

$$\rho_{\text{GJ}} = -\frac{\Omega \cdot \mathbf{B}_s}{2\pi c} \approx \pm \frac{B_s}{cP}, \quad (1)$$

where the positive/negative sign corresponds to ^{56}Fe ions/electrons. These two possibilities correspond to antiparallel and parallel relative orientation of the magnetic and spin axes, respectively. As mentioned before, there exists growing evidence (see Urpin & Gil 2004, and references therein) that the actual surface magnetic field B_s is highly non-dipolar. Its magnitude can be described in the form

$$B_s = bB_d \quad (2)$$

(Gil & Sendyk 2000, GS00 hereafter), where the enhancement coefficient $b > 1$ and

$$B_d = 2 \times 10^{12} (P \dot{P}_{-15})^{1/2} \text{ G} \quad (3)$$

is the canonical, star centered dipolar magnetic field, P is the pulsar period in seconds and $\dot{P}_{-15} = \dot{P}/10^{-15}$ is the period derivative. For the purpose of further considerations in this paper we introduce here a convenient measure of the surface magnetic field

$$\frac{B_s}{B_q} = 0.046 (P \dot{P}_{-15})^{0.5} b \quad (4)$$

where $B_q = 4.414 \times 10^{13}$ G is the so called quantum magnetic field (Erber 1966).

The polar cap is defined as the locus of the so-called open magnetic field lines that penetrate the light cylinder (GJ69). Generally, the polar cap radius can be written as

$$r_p = 1.45 \times 10^4 P^{-0.5} b^{-0.5} \text{ cm} \quad (5)$$

(GS00), where the factor $b^{-0.5}$ describes squeezing of the polar cap area due to the magnetic flux conservation in non-dipolar surface fields (as compared with the GJ69 dipolar configuration). One should realize, however, that the polar cap radius r_p expressed by the above equation is only a characteristic dimension. In fact, in the presence of strong non-dipolar surface magnetic field the actual polar cap can be quite irregular in shape. Also, the light-cylinder radius and thus the canonical polar cap radius depends on the unknown particle inertia (e.g. Michel 1973). Therefore, r_p as expressed in equation (5) can be used as an order of magnitude estimate of the actual polar cap radius.

The observationally deduced polar cap radii (see Section 3.2) are often much smaller than the canonical GJ69 value. This seems consistent with strong non-dipolar surface magnetic field, that is large b in equation (5). Given a strong enough near-surface magnetic field (the required condition will be discussed below in §§4-7), charge depletion in the acceleration region above the polar cap can result from binding of the positive $^{56}_{26}\text{Fe}$ ions (at least partially) in the neutron star surface. Positive charges then cannot be supplied at the rate that would compensate the inertial outflow through the light cylinder. As a result, a significant part of the unipolar potential drop (GJ69, RS75) develops above the polar cap, which can accelerate charged particles to relativistic energies and power the pulsar radiation. The characteristic height h of such an acceleration region is determined by the mean free path of pair-producing high energy photons. In other words, the growth of the accelerating potential drop is limited by the cascading production of an electron-positron plasma (e.g. RS75, CR80). The accelerated positrons would leave the acceleration region, while the electrons would bombard the polar cap surface, causing a thermal ejection of ions, which are otherwise more likely bound in the surface in the absence of additional heating. This thermal ejection would cause partial screening of the acceleration potential drop ΔV corresponding to a shielding factor

$$\eta = 1 - \frac{\rho_i}{\rho_{GJ}}, \quad (6)$$

where ρ_i is thermonically ejected charge density (see also eq.[18]) and

$$\Delta V = \eta \frac{2\pi}{cP} B_s h^2, \quad (7)$$

is the accelerating potential drop ⁴, where B_s is defined by equation (2) and h is the model dependent height of the acceleration region (see section 5). The above expression for ΔV is the solution of Poisson equation for a thin PSG, assuming that $\partial\eta/\partial h = 0$ within the acceleration region.

⁴In this paper we ignore slight reduction of ΔV due to general relativistic effect of frame dragging, which can affect the potential drop by as much as 27 percent (see Zhang et al. 2000; Gil & Melikidze 2002).

The cascading sparking discharge in PSG works analogously to the scenario envisioned by RS75. The only difference is that the accelerating potential drop is much smaller due to the partial screening by thermionic ions with charge density ρ_i . Additional positive charge density ρ_+ is supplied by the spark produced positrons. The potential drop is completely screened when the total charge density $\rho = \rho_i + \rho_+$ reaches the corotational value (eq.[1]). Then the spark plasma escapes from the region as discussed by Asseo & Melikidze (1998). However, during a short escaping timescale $h/c \sim 10^{-8}$ s the thermionic ions still maintain the partial screening as determined by equation (6). Thus, the returning potential drop quickly grows to the level defined by equation (7) and the spark begins to develop again. This results in an intrinsically intermittent nature of PSG and an unsteady particle flow into the magnetosphere, which has an important physical consequences for generation of the coherent pulsar radio emission (see section 8).

In the stationary observer's frame the co-rotational charge density $\rho_{GJ} = -\boldsymbol{\Omega} \cdot \mathbf{B}/2\pi c$ is associated with the co-rotational electric field $\mathbf{E}_{cor}(\mathbf{r}) = -(\boldsymbol{\Omega} \times \mathbf{r}) \times \mathbf{B}(\mathbf{r})/c$ and the magnetosphere co-rotates with the velocity $\mathbf{v}_{cor} = c(\mathbf{E}_{cor} \times \mathbf{B})/B^2$, where \mathbf{B} is the magnetic field (dipolar) and $\boldsymbol{\Omega}$ is the pulsar spin axis ($\Omega = 2\pi/P$). Now let us introduce a thin, charge depleted region extending to about h above the polar cap surface, with the accelerating potential drop described by equation (7). Since the charge density within this region is lower than the co-rotating value ρ_{GJ} , an additional electric field $\Delta\mathbf{E}$ appears in this region, which makes the spark plasma to drift with a velocity $\mathbf{v}_d = c/B^2(\Delta\mathbf{E} \times \mathbf{B})$, as observed in the co-rotating frame. To estimate the values of ΔE let us follow the original method of RS75 and consider the closed contour *abfea* within the gap, as marked in Figure 4 of RS75. Since the potential drop along segments *ab* and *bf* vanishes ($\Delta V_{ab} = \Delta V_{bf} = 0$), one then has $\Delta V_{ae} = \Delta V_{fe}$, where ΔV_{ae} corresponds to the tangent electric field $\Delta\mathbf{E}$, while ΔV_{ef} is just the acceleration potential drop expressed by equation (7). However, we can consider another segment *f'e'* (parallel to *fe*) and use the same argument to demonstrate that $\Delta V_{ae'} = \Delta V_{ae}$ for any arbitrary pair of points *e* and *e'*. This means that $\Delta E \approx 0$ within the RS75 gap, except at the boundary region within about h from the polar cap boundary, where h is the height of the gap. The perpendicular electric field ΔE grows rapidly from essentially zero to the corotational field \mathbf{E}_{cor} in the boundary region. The situation can be slightly different if the gap height h (length of segments *fe* and *f'e'*) varies between the pole and the polar cap edge, although in the thin gap case of RS75 ($h \ll r_p$) such variations cannot be large ($\Delta h/h \ll 1$). In this case $\Delta V_{fe} \neq \Delta V_{f'e'}$ and $\Delta V_{ae} \neq \Delta V_{ae'}$ and some residual ΔE can exist over the entire polar cap area. In any case, the tangent electric field is strong only at the polar cap boundary where $\Delta E = 0.5\Delta V/h = \eta(\pi/cP)B_s h$ (see Appendix A in GMG03 for details). Here B_s is the surface magnetic field (eqs. [3] and [2]), ΔV is the accelerating potential drop (eq. [7]), h is the gap height (eqs. [19] and [20]), and η is the shielding factor (eqs.[6], [9] and

[16]). This electric field causes that discharge plasma at the polar cap boundary performs a slow circumferential motion with velocity $v_d = c\Delta E/B_s = \eta\pi h/P$. The time interval to make one full revolution around the polar cap boundary is $\hat{P}_3 \approx 2\pi r_p/v_d$. One then obtains the so called tertiary drift periodicity

$$\frac{\hat{P}_3}{P} = \frac{r_p}{2\eta h}, \quad (8)$$

which is the proper measure of the intrinsic drift rate, at least at the boundary of the polar cap. If the plasma above the polar cap is fragmented into filaments (sparks) which determine the intensity structure of the instantaneous pulsar radio beam, then, at least in principle, the tertiary periodicity \hat{P}_3 can be measured/estimated from the pattern of the observed drifting subpulses (e.g. Deshpande & Rankin 1999; Gil & Sendyk 2003). In practice \hat{P}_3 is very difficult to measure (mainly because of aliasing which is a severe problem even in pulsars with high signal-to-noise ratio, e.g. DR99, GS03) and its value is known at the moment only in few cases. It is much easier to measure the primary drift periodicity P_3 , which in high signal-to-noise ratio is just a distance between the observed drift bands measured in pulsar periods P (there are also clever techniques that allow to measure P_3 even in cases with very low signal-to-noise ratio; see Edwards & Stappers 2002, WES06). Since $\hat{P}_3 = NP_3$ (e.g. RS75), where $N \approx 2\pi r_p/2h$ is the number of sparks contributing to the drifting subpulse phenomenon observed in a given pulsar (GS00), then one can write the shielding factor in the form

$$\eta \approx \frac{1}{2\pi} \frac{P}{P_3}, \quad (9)$$

which depends only on relatively easy-to-measure primary drift periodicity P_3 (WES06). This equation can be compared with the definition of shielding factor (eq.[6]) in order to derive the amount of thermally ejected iron ions or electrons (depending on the sign of charge of the polar cap). Apparently, the shielding parameter η should be much smaller than unity. Note that in the RS75 pure VG model one has $\eta = 1$, which implies the predicted subpulse drift at least an order of magnitude too fast as compared with observations. This means that the conditions within the natural inner acceleration region above the polar cap should greatly differ from the pure vacuum gap proposed by RS75.

3.1. Thermostatic self-regulation of the potential drop

GMG03 argued that because of the exponential sensitivity of the accelerating potential drop ΔV to the surface temperature T_s , the actual potential drop should be thermostatically regulated (see also CR80). In fact, when ΔV is large enough to ignite the cascading pair

production, the back-flowing relativistic charges will deposit their kinetic energy in the polar cap surface and heat it at a predictable rate. This heating will induce thermionic emission from the surface, which will in turn decrease the potential drop that caused the thermionic emission in the first place. As a result of these two oppositely directed tendencies, the quasi-equilibrium state should be established, in which heating due to electron bombardment is balanced by cooling due to thermal radiation. This should occur at a temperature T_s slightly lower than the critical temperature above which the polar cap surface delivers thermionic flow at the corotational (GJ69) charge density level (see GMG03 for more details).

The quasi-equilibrium condition is $\sigma T_s^4 = \gamma m_e c^3 n$, where $\gamma = e\Delta V/m_e c^2$ is the Lorentz factor and ΔV is the accelerating potential drop (eq. [7]). Here

$$n = n_{\text{GJ}} - n_i = \eta n_{\text{GJ}} \quad (10)$$

is the charge number density of back-flowing particles that actually heat the polar cap surface, η is the shielding factor (eq. [6]), n_i is the charge number density of thermally ejected flow and

$$n_{\text{GJ}} = \rho_{\text{GJ}}/e = 1.4 \times 10^{11} b \dot{P}_{-15}^{0.5} P^{-0.5} \text{ cm}^{-3} \quad (11)$$

(eq. [1]) is the corotational (GJ69) charge number density⁵. It is straightforward to obtain an expression for the quasi-equilibrium polar cap surface temperature in the form

$$T_s = (2 \times 10^6 \text{ K}) P^{-0.25} \dot{P}_{-15}^{0.25} \eta^{0.5} b^{0.5} h_3^{0.5}, \quad (12)$$

where $h_3 = h/10^3 \text{ cm}$ is the normalized height of the acceleration region. This height is model dependent and we discuss two possible models below (eqs. [21] or [22]). Growing evidence suggests that in actual pulsars T_s is few MK (see Table 1). Thus, from the above equation one can infer that $b \sim \eta^{-1}$, where the shielding parameter should be much lower than unity (see discussion below eq. [7]). As a consequence, the enhancement coefficient $b = B_s/B_d$ (eq. [2]) should be much larger than unity (at least of the order of 10). This is very consistent with the binding energy problem discussed in Section 4. Indeed, the extremely high surface magnetic field helps to resolve this problem.

3.2. Interrelationship between radio and X-ray signatures of drifting subpulses

The predicted thermal X-ray emission luminosity from the polar cap with temperature T_s is $L_x = \sigma T_s^4 A_{\text{bol}}$, where $A_{\text{bol}} = \pi r_p^2$ and r_p is the actual polar cap radius (eq. [5]) and

⁵Note that in the original RS75 paper the charge number density corresponds to purely dipolar magnetic field ($b = 1$), while in our approach the surface magnetic field is highly non-dipolar ($b \gg 1$).

σ is the Stefan-Boltzmann constant. Thus $L_x = 1.2 \times 10^{32} (\dot{P}_{-15}/P^3)(\eta h/r_p)^2$ erg/s, which can be compared with the spin-down power $\dot{E} = I\Omega\dot{\Omega} = 3.95 I_{45} \times 10^{31} \dot{P}_{-15}/P^3$ erg/s, where $I = I_{45} 10^{45}$ g cm² is the neutron star moment of inertia (in what follows we assume that $I_{45} = 1$). We can now use the equation (8) in the form $\eta h/r_p \approx 0.5P/\hat{P}_3$ and derive the thermal X-ray luminosity from the polar cap heated by sparks, i.e.

$$L_x = 2.5 \times 10^{31} \frac{\dot{P}_{-15}}{P^3} \left(\frac{\hat{P}_3}{P} \right)^{-2}, \quad (13)$$

where \hat{P}_3 is the tertiary periodicity in drifting subpulses pattern (pulsar carousel time), which is equal to the time interval needed for the discharge plasma to make one full revolution around the perimeter of the polar cap.

One can also derive the X-ray luminosity efficiency (with respect to the spin down luminosity)

$$\frac{L_x}{\dot{E}} = 0.63 \left(\frac{\hat{P}_3}{P} \right)^{-2}. \quad (14)$$

We can see that equations (13) and (14) depend only on the observational data of the radio pulsars. It is particularly interesting and important that both equations above do not depend on details of the sparking gap model (η, b, h). Thus, we have found a simple relationship between the properties of drifting subpulses observed in radio band and the characteristics of X-ray thermal emission from the polar cap heated by sparks associated with these subpulses. For PSR B0943+10, which is the only pulsar for which both $\hat{P}_3 = 37P$, (DR99) and $L_x = 5 \times 10^{28}$ erg s⁻¹ $\simeq 5 \times 10^{-4}\dot{E}$, (ZSP05) are measured, the above equations hold very well. In few other cases for which the circulational periodicity is measured $14 < \hat{P}_3/P < 37$ (see Table 1), which gives $L_x/\dot{E} \sim (1^{+4}_{-0.5}) \times 10^{-3}$. Such correlation between the X-ray and the spin-down luminosities is a well-known and intriguing property of rotation powered pulsars (Becker & Trümper 1997; Possenti, Cerratto, Colpi, et al. 2002). It has been suggested that this correlation is a characteristic of a magnetospheric radiation (e.g. Cheng, Gil, & Zhang 1998; Zhang & Harding 2000). Here we suggest that it can also be a characteristic property of the polar cap thermal radiation. Most likely, both mechanisms contribute at a comparable level to the observed X-ray luminosity. However, one should realize that if the estimates for PSRs 0809+74 and 0633+08 (Table 1) were correct, they would violate significantly the above correlation, so it should be treated with caution until confirmed or discarded.

Using equations (8) and (12) we can write the polar cap temperature in the form

$$T_s = (5.1 \times 10^6 \text{ K}) b^{1/4} \dot{P}_{-15}^{1/4} P^{-1/2} \left(\frac{\hat{P}_3}{P} \right)^{-1/2}, \quad (15)$$

where the enhancement coefficient $b = B_s/B_d \approx A_{\text{pc}}/A_{\text{bol}}$, $A_{\text{pc}} = \pi r_{\text{pc}}^2$ and $A_{\text{bol}} = \pi r_{\text{p}}^2$ (see Section 2). Since A_{bol} can be determined from the black-body fit to the spectrum of the observed thermal X-ray emission, the above equations can also be regarded as independent of details of the sparking gap model and depending only on the combined radio and X-ray data, similarly as equations (13) and (14). This seems quite understandable, since it reflects the simple fact that within the sparking gap model both the intrinsic drift rate and the polar cap heating rate are determined by the same electric field. Therefore, the observational values of L_x and \dot{P}_3/P should be related to each other through a combination of P and \dot{P} that is proportional to the spin-down power \dot{E} , as it is really so in equations (13) and (14). Let us summarize a set of assumptions that lead to these equations: (i) the electric field causing the drift is estimated at the polar cap boundary⁶ (eq. [8]), (ii) the gap is partially shielded (Eq.[10]), and (iii) the surface magnetic field at the polar cap is highly non-dipolar (eq. [11]). If some or all of these assumptions were not valid, then the unknown parameters such as h , b and/or η would appear in equations (13) and (14). Therefore, and observational verification of these equations seems to be an easy way to confirm or discard the PSG model of the inner accelerator in pulsars.

3.3. Actual pulsars

Table 1 presents the observational data and predicted values (computed from equations (13 - 15)) of a number of quantities for five pulsars, which we believe show clear evidence of thermal X-ray emission from spark heated polar caps. Besides the three cases with known \hat{P}_3 (B0943+10, B0826–34 and B0834+06), we also included PSR B1133+16 (twin of PSR B0943+10) for which we estimated \hat{P}_3 and argued that its value was actually measured but misinterpreted as the primary drift periodicity P_3 (shown in parenthesis in Table 1). PSR B0809+74, for which an estimate of \hat{P}_3 exists, is included. We also added the Geminga pulsar (B0633+17) for which thermal radiation from small polar cap was clearly detected.

PSR B0943+10. This is the best studied drifting subpulse radio pulsars with $P = 1.09$ s, $\dot{P}_{-15} = 3.52$, $\dot{E} = 10^{32}$ erg s⁻¹. DR99 clearly demonstrated that the observed subpulse drift is in this pulsar aliased and found the alias-resolved values of drift periodicities $\hat{P}_3 = 37.4P$ and $P_3 = 1.86P$, which gave the number of observed sparks $N = \hat{P}_3/P_3 = 20$. In an attempt to detect thermal X-ray signatures of these sparks ZSP05 observed this pulsar with the XMM-Newton. They obtained a spectrum consistent with thermal BB fit with a

⁶This is different from the original RS75 model, where the electric field is estimated at the middle of the polar cap. Moreover, they used pure vacuum gap model.

bolometric luminosity $L_x \approx 5 \times 10^{28} \text{ erg s}^{-1}$ and a polar cap surface area $A_{\text{bol}} = 10^7 (T_s/3 \times 10^6 \text{ K})^{-4} \text{ cm}^2 \sim (1_{-0.4}^{+4}) \times 10^7 \text{ cm}^2$, which was much smaller than the conventional polar cap area $A_{\text{pc}} = 6 \times 10^8 \text{ cm}^2$. This corresponds to the best fit temperature $T_s = 3.1 \times 10^6 \text{ K}$ (see Fig. 1 in ZSP05). The predicted values of L_x and L_x/\dot{E} calculated from equation (13) and (14), respectively, agree very well with the observational data. The surface temperature T_s calculated from equation (15) with $b = A_{\text{pc}}/A_{\text{bol}}$ is also in very good agreement with the best fit. The shielding parameter $\eta \approx 0.1$ is derived from equation (9).

PSR B1133+16. This pulsar with $P = 1.19 \text{ s}$, $\dot{P}_{-15} = 3.7$, and $\dot{E} = 9 \times 10^{31} \text{ erg s}^{-1}$ is almost a twin of PSR B0943+10. KPG05 observed this pulsar with Chandra and obtained a spectrum consistent with thermal BB fit $L_x = 6.7 \times 10^{28} \text{ erg s}^{-1}$ (we used their $L_x/\dot{E} = 3.6_{-0.7}^{+0.6} \times 10^{-4} < \cos \theta >^{-1}$ with $< \cos \theta > = 0.47$), $A_{\text{bol}} = (0.5_{-0.3}^{+0.5}) \times 10^7 \text{ cm}^2$ and $T_s \approx 2.8 \times 10^6 \text{ K}$. These values are also very close to those of PSR B0943+10, as should be expected for twins. Using equations (13) or (14) we can predict $\hat{P}_3/P = 27_{-2}^{+5}$ for B1133+16. Interestingly, Rankin (1986, R86 henceforth) gives the primary drift periodicity $P_3 = (5.3 \pm 1.2)P$ for the conal components (probably aliased), but in the saddle between these components R86 reports $P_3 = (25 \pm 3)P$. However, recently WES06, reported in this pulsar $P_3/P = 3 \pm 2$, as well as long period drift feature with $(33 \pm 3)P$ in the trailing profile component. We thus claim that this long period (shown in parenthesis in Table 1) is the actual tertiary periodicity $\hat{P}_3/P = 33_{-3}^{+3}$, which agrees very well with our prediction $\hat{P}_3/P = 27_{-2}^{+5}$. This interpretation is strongly supported by Fig. 10 in Nowakowski (1996), where the fluctuation spectrum of PSR B1133+16 shows prominent long period feature at 0.031 cycles/period, corresponding to 32 pulsar periods. It is worth noting that $\hat{P}_3/P_3 = 33 \pm 3$ is very close to 37.4 measured in the radio twin PSR B0943+10. Note also that the number of sparks predicted from our hypothesis is $N = \hat{P}_3/P_3 = (33 \pm 3)/(3 \pm 2) = 11_{-6}^{+25}$, thus it is quite possible that actually N is close to 20, as in the case of twin pulsar B0943+10.

PSR B0826–34. With $P = 1.85 \text{ s}$, $\dot{P}_{-15} = 1.0$, $\dot{E} = 6 \times 10^{30} \text{ erg s}^{-1}$, this pulsar has $P_3 \approx 1P$ (highly aliased) and $\hat{P}_3 \approx 14P$, i.e. $N = 14$ (Gupta, Gil, Kijak, et al. 2004; Esamdin, Lyne, Graham-Smith, et al. 2006). With these values we can predict from equation (13) that $L_x = 2 \times 10^{28} \text{ erg s}^{-1}$. This pulsar should be as bright as PSR B0943+10 and thus it is worth observing with *XMM-Newton*. The shielding parameter $\eta \approx 0.16$ (eq. [9]).

PSR B0834+06. With $P = 1.27 \text{ s}$, $\dot{P}_{-15} = 6.8$, and $\dot{E} = 1.3 \times 10^{32} \text{ erg s}^{-1}$, this pulsar has $\hat{P}_3 = 15P$, and $P_3 = 2.16 P$ (Asgekar & Deshpande 2005), implying the number of sparks $N \approx 15/2.16 \approx 7$. From equation (13) we obtain $L_x = 37 \times 10^{28} \text{ erg s}^{-1}$. This pulsar should be almost 8 times more luminous than PSR B0943+10, and we strongly recommend to observe it with *XMM-Newton*. The shielding parameter $\eta \approx 0.07$ (eq. [9]).

PSR B0809+74. This is one of the most famous pulsars with drifting subpulses, with $P = 1.29$ s, $\dot{P}_{-15} = 0.17$, $\dot{E} = 3.1 \times 10^{30}$ erg s $^{-1}$ and well determined value of the primary drift period $P_3 = 11 P$. Recently, van Leeven, Stappers, Ramachandran et al. (2003) estimated the circulatory tertiary period $\hat{P}_3 \geq 150P$. This is very long as compared with other pulsars considered above, but see the Geminga case below. Taking the lower limit $\hat{P}_3 = 150 P$ we can predict from eq. (13) thermal X-ray luminosity at the level $L_x = 3 \times 10^{25}$ erg s $^{-1}$, which is a very low compared with other nearby pulsars. The efficiency ratio $L_x/\dot{E} = 3 \times 10^{-6}$. The shielding factor $\eta = 0.014$ (eq. [9]).

PSR B0633+17 (Geminga). This pulsar with $P = 0.237$ s and $\dot{P}_{-15} = 10.97$ is a problematic radio emitter, but well known for pulsating optical, X-ray and Γ -ray emission. Recently, Caraveo, De Luca, Mereghetti et al. (2004) detected thermal emission from an 60 meter-radius polar cap heated to $T_s = (1.9 \pm 0.3) \times 10^6$ K, with the bolometric thermal luminosity $L_x = 1.5 \times 10^{29}$ erg s $^{-1}$. Since the canonical radius of the polar cap is 300 m, then the amplification factor $b(300/60)^2 = 25$ (eqs. [2] and [5]). Using the observed value of L_x we obtain from equation (13) the predicted value of $\hat{P}_3/P = 400$, which is even longer than the minimum estimate in PSR B0809+74. Now taking this value and the estimate for b we obtain from equation (15) $T_s = 2.13 \times 10^6$ K, which is in very good agreement with observational range of the surface temperature $(1.9 \pm 0.3) \times 10^6$ K. The efficiency ratio $L_x/\dot{E} = 4 \times 10^{-6}$, close to the estimate in PSR B0809+74.

Becker, Weisskopf, Tennant, et al. (2004) revealed the X-ray emission from a number of old rotation-powered pulsars. Among them is PSR B0823+26, which is well known to exhibit regularly drifting subpulses (see Table 1) with $P_3 = (2.2 \pm 0.2)P$ (WES06). Such an old drifting pulsar is an ideal case to study the spark associated thermal radiation from hot polar cap. Becker, Weisskopf, Tennant, et al. (2004) found an upper limit of the thermal contribution from a hot polar cap as being $T_{pc} = 1.17 \times 10^6$ K, which seems low as compared with estimates given in Table 1. However, Becker, Weisskopf, Tennant, et al. (2004) used a full canonical polar cap with radius 299 meters to estimate T_{pc} . In the actual non-dipolar surface magnetic field one should re-scale $T_s = b^{0.25}T_{pc}$, where $b = (r_p/r_{pc})^2 = B_s/B_d$ (eqs. [2,5]). Since $B_d = 10^{12}$ G in this case, b would be at least 10. This raises the lower limit of T_{pc} to be above 2×10^6 K, consistent with our model. The same applies to another old pulsar B0950+08 studied by Becker, Weisskopf, Tennant, et al. (2004).

4. Binding energy problem

The phenomenon of drifting subpulses seems to indicate strongly a presence of the charge depleted acceleration region just above the polar cap. However, the existence of such region

strongly depends on the binding energy of ^{56}Fe ions, which are the main building blocks of neutron star surface (Usov & Melrose 1995; Lai 2001). If this cohesive energy is large enough to prevent thermionic emission, a charge depleted acceleration region can be formed above the polar cap. Normally, at the solid-vacuum interface, the charge density of outflowing ions is roughly comparable with density of the solid at the surface temperature $kT_s = \varepsilon_c$, where ε_c is the cohesive (binding) energy and $k = 8.6 \times 10^{-8}$ keVK $^{-1}$ is the Boltzman constant. However, in the case of pulsars, only the corotational charge density ρ_{GJ} can be reached, and the ^{56}Fe ion number density corresponding to ρ_{GJ} is about $\exp(-30)$ times lower than in the neutron star crust. Since the density of outflowing ions ρ_i decreases in proportion to $\exp(-\varepsilon_c/kT_s)$, one can then write $\rho_i/\rho_{\text{GJ}} \approx \exp(30 - \varepsilon/kT_s)$. At the critical temperature

$$T_i = \frac{\varepsilon_c}{30k} \quad (16)$$

the ion outflow reaches the maximum value $\rho_i = \rho_{\text{GJ}}$ (Eq. [1]), and the numerical coefficient 30 is determined from the tail of the exponential function with an accuracy of about 10%.

Calculations of binding energies are difficult and uncertain (see Usov & Melrose 1995, 1996 and Lai 2001 for detailed discussion). In this paper we use the results of (Jones 1986, J86 henceforth), which were recommended by Lai (2001) in his review paper as more robust than others. J86 obtained $\varepsilon_c = 0.29, 0.60$ and 0.92 keV for $B_s = 2, 5$ and 10×10^{12} G, respectively. These values can be approximately represented by the function $\varepsilon_c \simeq (0.18\text{keV})(B_s/10^{12})^{0.7}$ G. Using equations (2), (3) and (16), this could be converted into the critical temperature

$$T_i \simeq (0.7 \times 10^5 \text{ K}) \left(\frac{B_s}{10^{12} \text{ G}} \right)^{0.7} \simeq (1.2 \times 10^5 \text{ K}) b^{0.7} (P\dot{P}_{-15})^{0.36} \approx (10^6 \text{ K}) \left(\frac{B_s}{B_q} \right)^{0.7}, \quad (17)$$

where we use the ratio B_s/B_q (eq. [4]) for the convenience of presenting the results in the graphical form (Fig. 1 and 2). Above this temperature the thermionic ion flow reaches the maximum GJ density at the surface, and the polar cap flow will be space charge limited. An acceleration potential can be still developed but the growth rate is slow compared with the PSG model we are developing in this paper. At temperatures below T_i charge-depletion would happen right above the surface, and an efficient acceleration region would form, which should be discharged in a quasi-steady manner by a number of sparks, similar to the original suggestion of RS75 for the pure vacuum gap case (see more detailed discussion in GMG03). The electron-positron plasma produced by sparking discharges co-exists with the thermally ejected ions, whose charge density can be characterized by the shielding factor (defined by eq. [6]) in the form

$$\eta = 1 - \exp \left[30 \left(1 - \frac{T_i}{T_s} \right) \right]. \quad (18)$$

As one can see from equations (6) and (18), at the temperature $T_i = T_s$ the shielding factor $\eta = 0$ (corresponding to fully developed space-charge limited flow with $\rho_i = \rho_{GJ}$), but even a very small drop of T_s below T_i , much smaller than 10%, corresponds to creation of the pure vacuum gap with $\eta = 1$ ($\rho_i = 0$). Thus, the condition for partially screened charge depleted acceleration region can be written in the form $T_s \lesssim T_i$, meaning that the actual surface temperature T_s should be slightly lower (few percent) than the critical ion temperature T_i , which for a given pulsar is determined purely by the surface magnetic field B_s (eq. [17]). Practically, one can use

$$T_s = T_i, \quad (19)$$

to denote the condition of forming a PSG, with the caveat that in reality T_s cannot be exactly equal to T_i but should be a few percent lower.

As mentioned above, the polar cap surface can be, in principle, negatively charged ($\mathbf{\Omega} \cdot \mathbf{B} > 0$). In such a case (called “antipulsars” by RS75) the polar cap surface can deliver an electron flow. Following GMG03 we assume that this electron flow is also determined mainly by thermoemission, with the corresponding shielding factor $\eta = 1 - \rho_e/\rho_{GJ} = 1 - \exp[25(1 - T_e/T_s)]$, where ρ_e is the charge density of thermionic electrons. The critical electron temperature is

$$T_e \simeq (5.9 \times 10^5 \text{ K}) b^{0.4} P^{0.16} \dot{P}_{-15}^{0.2} \sim (10^6 \text{ K}) \left(\frac{B_s}{B_q} \right)^{0.4} \quad (20)$$

(see GMG03 for more details), and in analogy to equation (19) the condition for creation of charge depleted acceleration region is $T_s = T_e$. Since the enhancement coefficient $b \gg 1$ (see the discussion following eq. [12]) so that $B_s/B_q \sim 1$ (eq. [4]), both T_i and T_e can be close to $T_s \sim$ a few MK. Since T_i and T_e are similar, we will only include the ion case (eq. [17]) in the following discussion, keeping in mind that our considerations are general and independent of the sign of the polar cap charge, at least qualitatively.

5. PSG models of the inner acceleration region in pulsars

So far, we have considered the macroscopic properties of the inner accelerator region in a way independent of details of the sparking gap model. Now we begin to discuss the microscopic properties of this model. In particular, we will present results of model calculations similar to those presented by GM02 but for a much larger sample of drifting subpulse pulsars and with the inclusion of partial screening due to thermionic emission from the polar cap surface. The condition for the formation of the gap used in GM02 was $T_c/T_s > 1$, while in this paper we used $T_c/T_s = 1$ (eq. [19]) as a result of the thermostatic regulation considered by GMG03.

Growth of the accelerating potential drop (eq. [7]) is limited by the cascading production of relativistic electron-positron pair plasma in strong and curved magnetic field. RS75 derived a famous formula for their VG height assuming that the quasi-steady breakdown is driven by magnetic pair production induced by the curvature radiation seed photons. They used Erber (1966) approximation, which is valid in relatively low magnetic fields $B_s/B_q \lesssim 0.1$, which is not relevant for the magnetic field at the polar cap considered in this paper. In the strong surface magnetic field, i.e. $B_s > 5 \cdot 10^{12}$ G, the high energy photons with energy $E_f = \hbar\omega$ produce electron-positron pairs at or near the kinematic threshold $\hbar\omega = 2mc^2/\sin\theta$, where $\sin\theta = l_{\text{ph}}/\mathcal{R}$, l_{ph} is the photon mean free path for pair formation and $\mathcal{R} = \mathcal{R}_6 \cdot 10^6$ cm is the radius of curvature of magnetic field lines. This regime is called the near threshold (NT) conditions (e.g. Daugherty & Harding 1983). Two VG models can be considered under the NT conditions: Curvature Radiation dominated Near Threshold Partially Screened Gap (CR-NTPSG) model and Inverse Compton Scattering dominated Near Threshold Partially Screened Gap (ICS-NTPSG) model, in which the potential drop is limited by pair production of the CR and the resonant ICS seed photons, respectively. Proper expressions corresponding to pure vacuum gap case have been derived by GM01 and GM02. Below we give generalized formulae by including partial screening due to the thermal flow from the polar cap surface (GMG03 and references therein).

CR-NTPSG model

In this model the cascading e^-e^+ pair plasma production is driven (or at least dominated) by the curvature radiation photons with typical energy $\hbar\omega = (3/2)\hbar\gamma^3c/\mathcal{R}$, where γ is the typical Lorentz factor of electrons/positrons moving relativistically along the local surface magnetic field lines with a radius of curvature \mathcal{R} . In the quasi-steady conditions the height h of the acceleration region is determined by the mean free path that is $h \sim l_{\text{ph}}$ for pair production by energetic CR photon in the strong and curved magnetic field. Following GM01 (see also GM02) and including the partial screening effect (GMG03) we obtain

$$h \approx h^{\text{CR}} = (3.1 \times 10^3)\mathcal{R}_6^{2/7}\eta^{-3/7}b^{-3/7}P^{3/14}\dot{P}_{-15}^{-3/14} \text{ cm.} \quad (21)$$

ICS-NTPSG model

In this model the cascading pair plasma production is driven (or at least dominated) by the resonant inverse Compton scattering (e.g. Zhang et al. 1997), with typical photon energy $\hbar\omega = 2\gamma\hbar e B_s/mc$. In the quasi-steady conditions the height h of the acceleration region is determined by the condition $h \sim l_e$ where $l_e = 0.0027\gamma^2(B_s/10^{12}\text{G})^{-1}(T_s/10^6 \text{ K})^{-1}$ is the mean free path of the electron to emit this high energy ICS photon (ZHM00), B_s is

the surface magnetic field and T_s is the actual surface temperature. Following GM01 and including partial screening (GMG03) we obtain

$$h \approx h^{\text{ICS}} = (5 \times 10^3) \mathcal{R}_6^{4/7} \eta^{-1/7} b^{-1} P^{-5/14} \dot{P}_{-15}^{-1/2} \text{ cm.} \quad (22)$$

In the above equations $\mathcal{R}_6 = \mathcal{R}/10^6$ cm is the normalized curvature radius of the surface magnetic field lines.

Besides resonant ICS, also the non-resonant ICS with a characteristic energy $\hbar\omega \sim \max(\gamma^2 kT, \gamma mc^2)$ has been widely discussed in literature. This process usually dominates the gap dynamics in pulsars with moderate and low magnetic fields (Zhang et al. 1997; Hibschman & Arons 2001; Harding & Muslimov 2002). Since the polar caps in our model typically anchor a very strong curved magnetic field, the non-resonant ICS is unimportant and we ignore it in our detailed treatment. Throughout this paper ICS refers to resonant ICS, and the equations (21) and (22) will be referred as to CR and ICS cases, respectively.

5.1. CR-NTPSG

The results of model calculations for 102 pulsars with drifting subpulses (see Table 1) are presented in Figure 1 for the ion T_i critical temperature (eq. [17]). We have plotted B_s/B_q (left-hand side vertical axes) versus the pulsar number (which corresponds to a particular pulsar according to Table 1). The actual value of B_s/B_q (eq. [4]) for a given pulsar was computed from the condition $T_s = T_i$, where T_s is the actual surface temperature (eq. [12]), with the height h of CR driven acceleration region determined by equation (21). This condition leads to the expression $B_s/B_q = 126.4 P^{-20/29} \mathcal{R}_6^{10/29} \eta^{20/29}$, which allows to sort pulsars according to decreasing value of pulsar period P , which is marked on the top of the Figure 1. The vertical axes on the right hand side are expressed in terms of the surface temperature T_s computed from equation (17). Different panels correspond to different normalized radii of curvature ranging from $\mathcal{R}_6 = 0.1$ to $\mathcal{R}_6 = 0.009$. Different symbols used to plot exemplary curves correspond to arbitrarily chosen values of shielding factor ranging from $\eta = 0.015$ to $\eta = 0.15$ (each curve represents the same shielding conditions η for all 102 pulsars considered).

The vertical line in Figure 1 corresponds to PSR B0943+10 (N1=41 in Table 1), which was observed using XMM-Newton by ZSP05. Three horizontal lines correspond to T_s equal to about 2, 3 and 4 MK (from bottom to the top), respectively, calculated from equation (17). (More exactly, we marked $T_s = T_i = 2.08, 3.11$ and 4.14 for $B_s/B_q = 2.7, 4.8$ and 7.2 , respectively). Thus, the hatched areas encompassing these lines correspond to the range of surface temperatures $T_s \cong (3 \pm 1) \times 10^6$ K deduced observationally for the polar cap of

B0943+10 from XMM-Newton observations (ZSP05, see their Fig. 1).

5.2. ICS-NTPSG model

Let us now consider the resonant inverse Compton scattering radiation model (ICS-NTPSG). The major difference between CR and ICS cases is the additional regulation of T_s caused by the condition $h \approx l_e$, where l_e is inversely proportional to T_s . In fact, the increase of the surface temperature causes the decrease of h , and hence, the decrease of ΔV . This makes the back-flow heating of the polar cap surface less intense. Let us estimate the surface temperature in the ICS dominated case. The average Lorentz factor of electrons or positrons can be estimated by the gap height and the partially screened potential drop as $\gamma = (1.1 \times 10^2) P^{1/6} \dot{P}_{-15}^{-1/6} b^{1/3} (T_s/10^6)^{2/3} \eta^{-1/3}$. Using the kinematic near threshold condition and the expression of the resonant ICS photons energy (see section 2) we get $\hbar\omega = (7.5 \times 10^{-8}) \gamma b (P \dot{P}_{-15})^{-1/2}$, which leads to another estimate for the average Lorentz factor $\gamma = 2.5 (T_s/10^6)^{1/3} \mathcal{R}_6^{1/3}$. Combining these two expressions for γ we find that for the case of the ICS dominated NTPSG the following relationship should hold $\eta = 8.14 \times 10^{-5} P^{1/2} \dot{P}_{-15}^{-1/2} b (T_s/10^6) \mathcal{R}_6^{-1}$. As a result, contrary to the CR case, the shielding factor η is not a free parameter in the ICS case, and the analysis similar to that presented in Figure 1 is not relevant. However, we can use the quasi-equilibrium condition $\sigma T_s^4 = \gamma m_e c^3 n_0 \eta$, which leads to $T_s = (8.8 \times 10^4) \left(\gamma \eta b P^{-3/2} \dot{P}_{-15}^{-1/2} \right)^{1/4}$. Using the expressions of η and γ we can then obtain

$$T_s = (1.5 \times 10^4 \text{ K}) \mathcal{R}_6^{-1/4} P^{-3/8} \dot{P}_{-15}^{-3/8} b^{3/4}. \quad (23)$$

Consequently, we can obtain the expression for the shielding factor

$$\eta = (1.2 \times 10^{-6}) P^{1/8} \dot{P}_{-15}^{-7/8} \mathcal{R}_6^{-5/4} b^{7/4}. \quad (24)$$

Thus, for a given pulsar (P, \dot{P}) the values of T_s and η are determined by the parameters of the local surface magnetic field \mathcal{R}_6 and b . In Figure 2 we plot T_s as a function of B_s/B_q (eq. [4]) for different values of \mathcal{R}_6 and η . The smooth lines in both panels correspond to the ion critical temperature, while other lines marked by different symbols shown in legends correspond to the actual surface temperature calculated for the CR case (upper panel) and the ICS case (lower panel). We look for partially screened solutions corresponding to the intersection of smooth and symbol-broken lines.

As seen from the lower panel of Figure 2, equations (23) and (24) cannot be self-consistently satisfied. In fact, unlike in the CR case presented in the upper panel, in the ICS case the surface temperature $T_s \simeq 10^6 \text{ K}$ (eq. 23) is considerably lower than T_i (eq. 17).

Bringing T_s close to T_i would imply $\eta = 1$ (pure vacuum), which is inconsistent with equation 24. Thus, if the pair creation is controlled by ICS, then the acceleration region should be a pure vacuum gap rather than a PSG. This is consistent with previous results of GM02, who concluded that in the pure vacuum gap case ICS seed photons are more efficient in driving the cascading pair production. However, GM02 failed to understand that CR pair production mechanism produces more polar cap heating and thus makes the gap partially screened. In such a case the ICS pair production still occurs but it is no longer the dominant mechanism to control the properties (height, potential drop, etc) of the acceleration region above the polar cap.

6. Thermal signatures of hot polar cap

Knowing that ICS cannot contribute significantly to the pair production process in a PSG, let us consider polar cap heating by back-flow plasma particles created from CR seed photons. Using the near threshold condition in the form $h = (4/3)(mc\mathcal{R}^2/\hbar\gamma^3) = h_3 10^3$ cm (see below eq. [4]) we can rewrite equation (12) in the form

$$T_s = (7.7 \times 10^6 \text{ K}) P^{-2/7} \eta^{2/7} \mathcal{R}_6^{1/7} \left(\frac{B_s}{B_q} \right)^{2/7}. \quad (25)$$

Consequently, we can obtain efficiency of thermal X-ray emission in the form

$$\frac{L_x}{\dot{E}} = 0.15 P^{19/14} \dot{P}_{-15}^{-1/2} \eta^{8/7} \mathcal{R}_6^{4/7} \left(\frac{B_s}{B_q} \right)^{1/7}, \quad (26)$$

where $L_x = \sigma T_s A_{\text{bol}}$ is the X-ray luminosity from the hot polar cap with the surface area $A_{\text{bol}} = \pi r_p^2$ (eq. [5]) and $\dot{E} = I\Omega\dot{\Omega} = 3.95 \times 10^{31} \dot{P}_{-15}/P^3$ erg/s is the spin-down power. For the twin radio pulsars PSR B0943+10 and PSR B1133+16 the X-ray signatures of the hot polar cap are $T_s \sim 3 \times 10^6$ K, $\dot{E} \approx 10^{32}$ erg/s and $L_x/\dot{E} \sim 5 \times 10^{-4}$ (see Table 1). Using these measurements we can infer from equations (25) and (26) an approximate condition in the form $\eta^2 \mathcal{R}_6 \sim 6.5 \times 10^{-5}$. Since in PSR B0943+10 $P_3/P = 1.86$ then according to equation (9) we obtain the normalized radius of curvature $\mathcal{R}_6 = 0.009$ in this pulsar (see next section). The microscopic equations (26) and (26) along with two macroscopic equations (14) and (15) provide full knowledge about the spark driven inner acceleration regions in pulsars. The PSG model behind these equations should be easily verifiable because they are either completely independent or weakly dependent on physical parameters of the acceleration region.

Figures 3 and 4 present calculations of the efficiency L_x/\dot{E} and the temperature T_s , respectively, for 102 pulsars from Table 1. One should emphasize that these calculations

utilized the two above equations and did not assume a priori an existence of the PSG in form of the condition $T_s = T_c$ (eqs. [17] and [19]). Thus, these figures should be considered in association with Figure 1, which does take into account this condition. The vertical solid lines correspond to PSR B0943+10 for which $T_s = (3 \pm 1) \times 10^6$ K (corresponding to $B_s/B_q = 4.8$ in Fig. 1) and $L_x/\dot{E} = (5 \pm 2) \times 10^{-4}$ (ZSP05). Due to weak dependence of the efficiency on the magnetic field we decided to use only one value of $B_s/B_q = 4.8$ in Figure 3 to avoid overlapping of too many lines. The observational range of L_x/\dot{E} and T_s are marked by the hatched belts in Figure 3 and 4, respectively. Since L_x/\dot{E} in equation (26) depends on both P and \dot{P} we have sorted pulsars in Figure 3 according to increasing value of \dot{E} , which are marked on the top of the figure (N2 in Table 1). If $L_x/\dot{E} \sim 10^{-3} \div 10^{-4}$ for all pulsars, then one can say that the shielding factor η should be larger for pulsars with larger \dot{E} . Also, it follows from Figure 4 that if $T_s = (2 \div 4) \times 10^6$ K in all pulsars, then the shielding factor η should be larger for longer period pulsars. This is consistent with equation (9).

7. Special case of PSR B0943+10

The microscopic parameters of PSR B0943+10 are described in section 3.2 (with appropriate entry in Table 1). Let us now discuss this special case in more detail. PSR B0943+10 is the only pulsar for which both \hat{P}_3 and L_x are known observationally. As already mentioned above, both the subpulse drift rate and the polar cap heating rate (due to subpulse-producing sparks) are related to the same value of the accelerating potential drop. In section 3, we found a “clear cut” formula involving two observables: the X-ray luminosity L_x and the tertiary drift periodicity \hat{P}_3 , which is independent of microscopic details of the acceleration region. This relationship holds very well for PSR B0943+10 (see Table 1). It is important to check whether this “model independent” approach is consistent with detailed model calculations, involving microscopic conditions prevailing in PSG. According to equations (8) and (9) we have the shielding parameter $\eta = 0.09$ and the complexity parameter $r_p/h = N/\pi = 6.36$, in consistency with GS00 (see also Gil, Melikidze, & Mitra 2002). Let us analyze in this respect our Figure 1, which allows to read off the physical parameters of the acceleration region for a given pulsar within a particular model η . For PSR B0943+10, only the intersections of the vertical lines corresponding to N1=41 (see Table 2) with the hatched belts, or even with the horizontal line $T_s = 3\text{MK}$, are relevant. The above value of $\eta = 0.09$ corresponds to the radius of curvature $\mathcal{R}_6 \sim 6.5 \times 10^{-5} \eta^{-2} \sim 0.009$ (see the condition below eq. [26]), and thus from the lower-right panel of Figure 1 we have $B_s/B_q \sim 5$ or $B_s \sim 2 \times 10^{14}$ G and $T_s \sim 3 \times 10^6$ K. This set of parameters can be also inferred from the upper panel in Figure 2. These values therefore are consistent with the appropriate entry for PSR B0943+10 in Table 1. This consistency between macro- and micro-scopic calculations

holds also for other pulsars from Table 1, as illustrated in Figure 3. This set of parameters can be also inferred from the upper panel in Figure 2.

The surface temperature about 3MK (ZSP05), which implies $B_s = bB_d \sim 2 \times 10^{14}$ G if one applies J86 theory (eq. [17]) to the case of B0943+10. The value exceeding 10^{14} G may seem extremely high, but at least three radio pulsars have dipolar magnetic fields above 10^{14} G (McLaughlin et al. 2003, and references therein). The non-dipolar surface magnetic fields could be even stronger. The reason that the inferred non-dipolar field is even stronger than in the pure vacuum case found in GM02 for the ICS seed photons is that we are using a lower binding energy calculations of Jones (1986), which are more robust than those of Abrahams & Shapiro (1991) (see Lai 2001, for critical review). However, generally the surface magnetic field required to form CR-NTVG obtained by GM02 is still higher than that for CR-NTPSG obtained in this paper.

In section 3.1 we assumed a pure black-body conditions at the polar cap. GM02 considered deviations from the black-body conditions by introducing the so-called heat-flow coefficient $\kappa = Q_{rad}/(Q_{rad} + Q_{cond})$, which described the amount of heat conducted beneath the polar cap that cannot be transferred back to the surface during the spark development time scale (see Appendix B in GM02). The heat flow coefficient κ influenced the required surface magnetic field B_s in proportion to $\kappa^{0.57}$ (for CR case). GM02 argued that for $T_s \sim 1$ MK this effect could reduce the required B_s by a factor of about 2. However, if $T_s \sim 3$ MK as indicated by the case of PSR B0943+10, the reduction effect is negligible and we ignored it in this paper.

8. Discussion and Conclusions

The phenomenon of drifting subpulses has been widely regarded as a powerful tool for understanding the mechanism of coherent pulsar radio emission. RS75 first proposed that drifting subpulses are related to $\mathbf{E} \times \mathbf{B}$ drifting sparks discharging the high potential drop within the inner acceleration region above the polar cap. The subpulse-associated streams of secondary electron-positron plasma created by sparks were penetrated by much faster primary beam. This system was supposed to undergo a two-stream instability, which should lead to generation of the coherent radiation at radio wave lengths. However, careful calculations of the binding energy (critical for spark ignition) and the growth rate of the two-stream instability have shown that neither the sparking discharge nor the two-stream instability were able to work in a way proposed by RS75. Nonetheless, qualitatively their idea was still considered attractive, at least to the authors of this paper who have been continuing efforts to search for mechanisms that would actually make the RS75 model to work. In this

paper we applied the partially screened gap model proposed by GMG03 to PSR B0943+10, a famous drifter for which ZSP06 successfully attempted to measure the thermal X-ray from hot polar cap. We derived a simple relationship between the X-ray luminosity L_x from the polar cap heated by sparks and the tertiary periodicity \hat{P}_3 of the spark-associated subpulse drift observed in radio band. This relationship reflects the fact that both the drifting (radio) and the heating (X-rays) rates are determined by the same value of the electric field in the partially screened gap. As a consequence of this coupling equations (13) and (14) are independent of details of the acceleration region. In PSRs B0943+10 and B1133+16, the only two pulsars for which both L_x and \hat{P}_3 are measured, the predicted relationship between observational quantities holds very well. We note that \hat{P}_3 is very difficult to measure and its value is known only for four pulsars: B0943+10, B1133+16, B0826–34 and B0834+06. The successful confrontation of the predicted X-ray luminosity with the observations in PSRs B0943+10 and B1133+16 encourages further tests of the model with future X-ray observations of other drifting pulsars. This is particularly relevant to PSR B0834+06, whose predicted X-ray luminosity is much higher than in PSR B0943+10, while the distance to both pulsars is almost identical. It is worth mentioning that due to relatively poor photon statistics it is still not absolutely clear whether the X-ray radiation associated with polar cap of PSR B0943+10 is thermal or magnetospheric (or both) in origin. However, the case of Geminga pulsar B0633+17 strongly supports thermal origin. Observations of PSR B0834+06 with *XMM-Newton* should help to resolve this question ultimately.

In both the steady SCLF model and the pure vacuum gap model, the potential increases with height quadratically at lower altitudes. However the growth rate is significantly different - the latter is faster by a factor of R/r_p . It is well known that in the pure vacuum case (RS75), the potential grows so fast that a primary particle could quickly generate pairs with a high multiplicity, and that some backward returning electrons generate more pairs and soon a “pair avalanche” occurs and the potential is short out by a spark. In the PSG model we are advocating, the potential drops by a factor of η . For essentially all the cases we are discussing, this η value is much larger than the r_p/R value required for the steady SCLF to operate, although it is much less than unity. The steady state condition is not satisfied, and the the gap is more analogous to a vacuum gap, i.e. the pair discharging happening intermittently. In fact, the partially screened potential drop is still above the threshold for the magnetic pair production, which in strong and curved surface magnetic field is a condition necessary and sufficient for the sparking breakdown.

The original RS75 pure VG model predicts much too high a subpulse drift rate and an X-ray luminosity to explain the case of PSR B0943+10 and other similar cases. Other available acceleration models predict too low a luminosity and the explanation of drifting subpulse phenomenon is generally not clear at all (see ZSP05 for more detailed discussion).

In summary, the bolometric X-ray luminosity for the space charge limited flow (Arons & Scharlemann 1979) pure vacuum gap (RS75) and partially screened gap (GMG03) is $(10^{-4} - 10^{-5})\dot{E}$ (Harding & Muslimov 2002), $(10^{-1} - 10^{-2})\dot{E}$ (ZSP05), and $\sim 10^{-3}\dot{E}$ (this paper), respectively. The latter model also predicts right $\mathbf{E} \times \mathbf{B}$ plasma drift rate. Thus, combined radio and X-ray data are consistent only with the partially screened VG model, which requires very strong (generally non-dipolar) surface magnetic fields. Observations of the hot-spot thermal radiation almost always indicate bolometric polar cap radius much smaller than the canonical Goldreich-Julian value. Most probably such a significant reduction of the polar cap size is caused by the flux conservation of the non-dipolar surface magnetic fields connecting with the open dipolar magnetic field lines at distances much larger than the neutron star radius.

Our analysis suggests the following pulsar picture: In the strong magnetic fields approaching 10^{14} G at the neutron star surface, the binding energy is high enough to prevent a full thermionic flow from the hot polar cap at the corotation limited level. A partially screened vacuum gap develops with the acceleration potential drop exceeding the threshold for the magnetic pair formation. The growth of this potential drop should be naturally limited by a number of isolated electron-positron spark discharges. As a consequence, the polar cap surface is heated by back-flowing particles to temperatures $T_s \sim 10^6$ K, just below the critical temperature T_c at which the thermionic flow screens the gap completely. The typical radii of curvature of the field lines \mathcal{R} is of the order of polar cap radii $r_p \sim 10^3 - 10^4$ cm. The only parameter that is thermostatically adjusted in a given pulsar is the shielding parameter $\eta = 10^{-3}(B_s/B_q)\mathcal{R}_6^{-0.5}P \sim 0.001T_6^{1.43}\mathcal{R}_6^{-0.5}P$, which determines the actual level of charge depletion with respect to the pure vacuum case ($\eta=1$), and in consequence the polar cap heating rate as well as the spark drifting rate. It is worth to emphasize that $\eta \sim 0.1$ for longer period pulsars $P \sim 1$ s and $\eta \sim 0.01$ for shorter period pulsars. Our calculations are consistent with PSR B0943+10 and few other drifting pulsars, for which the signatures of X-ray emission from the hot polar cap were detected.

The sparks operating at the polar cap generate streams of secondary electron-positron plasma flowing through the magnetosphere. These streams are likely to generate beams of coherent radio emission that can be observed in the form of subpulses. Usov (1987) first pointed out that the non-stationarity associated with sparking discharges naturally leads to a two-stream instability as the result of mutual penetration between the slower and the faster plasma components. Asseo & Melikidze (1998) developed this idea further, calculated the growth rates, and demonstrated that the instability is very efficient in generating Langmuir plasma waves at distances of many stellar radii $r_{\text{ins}} \sim 10^{4-5}h^{CR} = 10^{7-8}$ cm, where h^{CR} is the height of the acceleration region described by equation (21) (Melikidze, Gil & Pataraya 2000). This is exactly where pulsar's radio emission is supposed to originate (e.g. Kijak, & Gil

1998). Conversion of these waves into coherent electromagnetic radiation escaping from the pulsar magnetosphere was considered and discussed by Melikidze, Gil & Pataraya (2000) and Gil, Lyubarski, & Melikidze (2004). These authors demonstrated that the nonlinear evolution of Langmuir oscillations developing in pulsar's magnetosphere leads to formation of charged, relativistic solitons, able to emit coherent curvature radiation at radio wavelengths. The component of this radiation that is polarized perpendicularly to the planes of dipolar magnetic field can escape from the magnetosphere (see Lai et al. 2001, for observational evidence of such polarization of pulsar radiation). The observed pulsar radiation in this picture is an indirect consequence of sparking discharges within the inner acceleration region just above the polar cap. In light of this paper we can therefore argue that the coherent pulsar radio emission is conditional on the presence of strong non-dipolar surface magnetic fields at the polar cap, with a strength about 10^{13-14} G and radius of curvature of the order 10^4 cm.

In the very strong surface magnetic field assumed within the accelerator, processes such as photon splitting (Baring & Harding 2001) and bound pair creation (Usov & Melrose 1995) may become important. It has been suggested that such processes could potentially delay pair creation and thus increase the height and voltage of the accelerator. For the photon splitting case, the delay is significant only if photons with both polarization modes split - a hypothesis in strong magnetic fields (Baring & Harding 2001). It could be possible that only one mode split (Usov 2002). In such a case the gap height and potential of a PSG would not be significantly affected due to the high pair multiplicity in strong, curved magnetic fields. For bound pairs (Usov & Melrose 1995, 1996), in the very hot environment near the neutron star surface (with temperatures exceeding 1 MK), it is possible that bound pairs could not survive long from photoionization. Following Bhatia, Chopra, & Panchapakesan (1992) and Usov & Melrose (1996) one can roughly estimate the mean free path for bound pair photoionization. It turns out that for temperatures around (2-3) MK this mean free path is of the order of few meters, which is considerably less than the height of CR-driven PSG. In such a case, even if the bound pairs are initially produced, they would not significantly delay the pair formation. One could address this potential potential problem by referring to the detailed case study of PSR B0943+10 analyzed in this paper. This is the only pulsar in which we have full information concerning $\mathbf{E} \times \mathbf{B}$ drift rate and the polar cap heating rate. In the analysis we have used two methods. The first method is independent on details of accelerating region (such as height, potential drop, etc.) but is based only on the subpulse drift radio-data (eqs. [13,14]). The second one includes the detailed treatments of model parameters without considering the delaying effect by photon splitting and bound pairs (eqs. [25,26]). Both methods give consistent results, as illustrated in Figures (1-4). We therefore conclude that the delaying processes, if any, are not significant in the PSGs given

the physical conditions we invoke. Finally, we note that Usov & Melrose (1995) presented a model of the inner accelerator that shares some similar features with our model, although it is basically different. In their model the potential drop is self-regulated by partial screening close to the threshold for field ionization of bound pairs, so the surface temperature is maintained at the level necessary for this screening. In our model, the partial screening keeps the surface temperature slightly below the critical temperature at which the thermionic flow is space charge limited Arons & Scharlemann (1979). In the light of results presented in this paper we claim that bound pairs do not affect the formation of inner accelerators in pulsars.

We acknowledge the support of the Polish State Committee for scientific research under Grant 2 P03D 029 26 (JG & GM) and NASA grants NNG05GB67G, NNG05GH91G and NNG05GH92G (BZ).

REFERENCES

Abrahams, A.M., & Shapiro, S.L. 1991, *ApJ*, 374, 652

Arons, J. & Scharlemann, E. T. 1979, *ApJ*, 231, 854

Arons, J. 2001, *MNRAS*, 326, 1249

Asgekar, A., Deshpande,A. 2001, *MNRAS*, 326, 1249

Asgekar, A., Deshpande,A. 2005, *MNRAS*, 357, 1105

Asseo, E., & Melikidze,G.I. 1998, *MNRAS*, 301, 59

Backer, D.C., 1976, *ApJ*, 209, 895

Baring, M. G. & Harding, A. K. 2001, *ApJ*, 547, 929

Becker, W., Trümper, J., 1997, *A&A*, 326, 682

Becker, W., Weisskopf, M. C., Tenant, A. F., Jessner, A., Dyks, J., Harding, A. K., Zhang, S. N. 2004, *ApJ*, 615, 908

Bhatia,V.B., Chopra, N., & Panchapakesan, N., 1992, *ApJ*, 388, 131

Caraveo, P.A., De Luca, A., Mereghetti, S. et al. 2004, *Science* 305, 376

Cheng A.F., Ruderman M.A., 1980, *ApJ*, 235, 576 (CR80)

Cheng K.S., Gil J., & Zhang L., 1998, *ApJ*, 493, L35

Daugherty J., Harding A.K., 1983, *ApJ*, 273, 761

Deshpande, A.A., & Rankin, J.M. 1999, *ApJ*, 524, 1008 (DR99)

Deshpande, A.A., & Rankin, J.M. 2001, *MNRAS*, 322, 438 (DR01)

Edwards, R.I., & Stappers, B.B., 2002, *A&A*, 393, 733

Erber, T. 1966, *Rev. Mod. Phys.*, 38, 626

Esamdin, A., Lyne, A.G., Graham-Smith, F., et al. 2005, *MNRAS*, 356, 59

Fung, P.K., Khechinashvili, D., & Kuijpers, J. 2006, *A&A*, 445, 779

Geppert, U., Reinhardt, M., & Gil, J. 2003, *A&A*, 272, 268

Gil, J., Kijak, J., & Seiradakis, J. 1993, *A&A*, 272, 268

Gil J., & Mitra D., 2001, *ApJ*, 550, 383 (GM01)

Gil J. & Melikidze G.I., 2002, *ApJ*, 577, 909 (GM02)

Gil, J., Melikidze, G.I., & Mitra, D. 2002, *A&A*, 388, 246

Gil J., Melikidze G.I., & Geppert U., 2003, *A&A*, 407, 315 (GMG03)

Gil, J., Lyubarski, Yu., & Melikidze, G.I. 2004, *ApJ*, 600, 872

Gil, J., & Sendyk, M., 2000, *ApJ*, 541, 351 (GS00)

Gil, J., & Sendyk, M. 2003, *ApJ*, 585

Gogobaridze, G., Machabeli, G.Z., Merlose, D.B., & Luo, G. 2005, *MNRAS*, 360, 669

Goldreich P., & Julian H., 1969, *ApJ*, 157, 869 (GJ69)

Gupta, Y., Gil, J., Kijak, J., et al. 2004, *A&A*, 426, 229

Harding, A. K., & Muslimov, A. G. 1998, *ApJ*, 508, 328

Harding, A. K. & Muslimov, A. G. 2002, *ApJ*, 568, 862

Hibschman, J. A. & Arons, J. 2001, *ApJ*, 554, 624

Jones P.B., 1986, *MNRAS*, 218, 477 (J86)

Kazbegi, A. Z., Machabeli, G. Z., & Melikidze, G. I. 1991, Australian J. Phys., 44, 573

Kijak, J., & Gil, J. 1998, MNRAS, 299, 855

Lai D., 2001, Rev. Mod. Phys., 73, 629

Lai, D., Chernoff, D. F., & Cordes, J. M. 2001, ApJ, 549, 1111

Lyne, A.G., & Manchester, R.N., 1988, MNRAS, 234, 477

McLaughlin M.A., Stairs, I.H., Kaspi, V.M., et al., 2003, ApJ, 591, L135

Melikidze, G.I., Gil, J.A., & Pataraya, A.D., 2000, ApJ, 544, 1081

Nowakowski, L., 1996, ApJ, 457, 868

Possenti A., Cerratto R., Colpi M., et al., 2002, A&A, 387, 993

Rankin J.M., 1986, ApJ, 301, 901 (R86)

Ruderman M.A., Sutherland P.G., 1975, ApJ, 196, 51 (RS75)

Spitkovsky, A, Arons, J. 2002, ASPC, 271, 81

Urpin V., & Gil J., 2004, A&A, 415, 356

Usov, V.V. 1987, ApJ, 320, 333

Usov, V. V. 2002, ApJ, 572, L87

Usov, V.V., & Melrose, D.B., 1995, Ast. J. Phys., 48, 571

Usov, V.V., & Melrose, D.B., 1996, ApJ, 464, 306

Weltevrede P., Edwards R.I., & Stappers B.A., 2006, A&A, 445, 243

Wright, G. A. E. 2003, MNRAS, 344, 1041

Zhang B., Harding A., & Muslimov A., 2000, ApJ, 531, L135

van Leeven, A.G.J., Stappers, B.W., Ramachandran, R. et al., A&A, 2003, 399, 223

Zhang B., Sanwal D., & Pavlov G.G., 2005, ApJ, 624, L109 (ZSP05)

Zhang, B., Qiao, G. J., Lin, W. P. & Han, J. L. 1997, ApJ, 478, 313

Zhang, B., & Harding, A. 2000, ApJ, 532, 1150

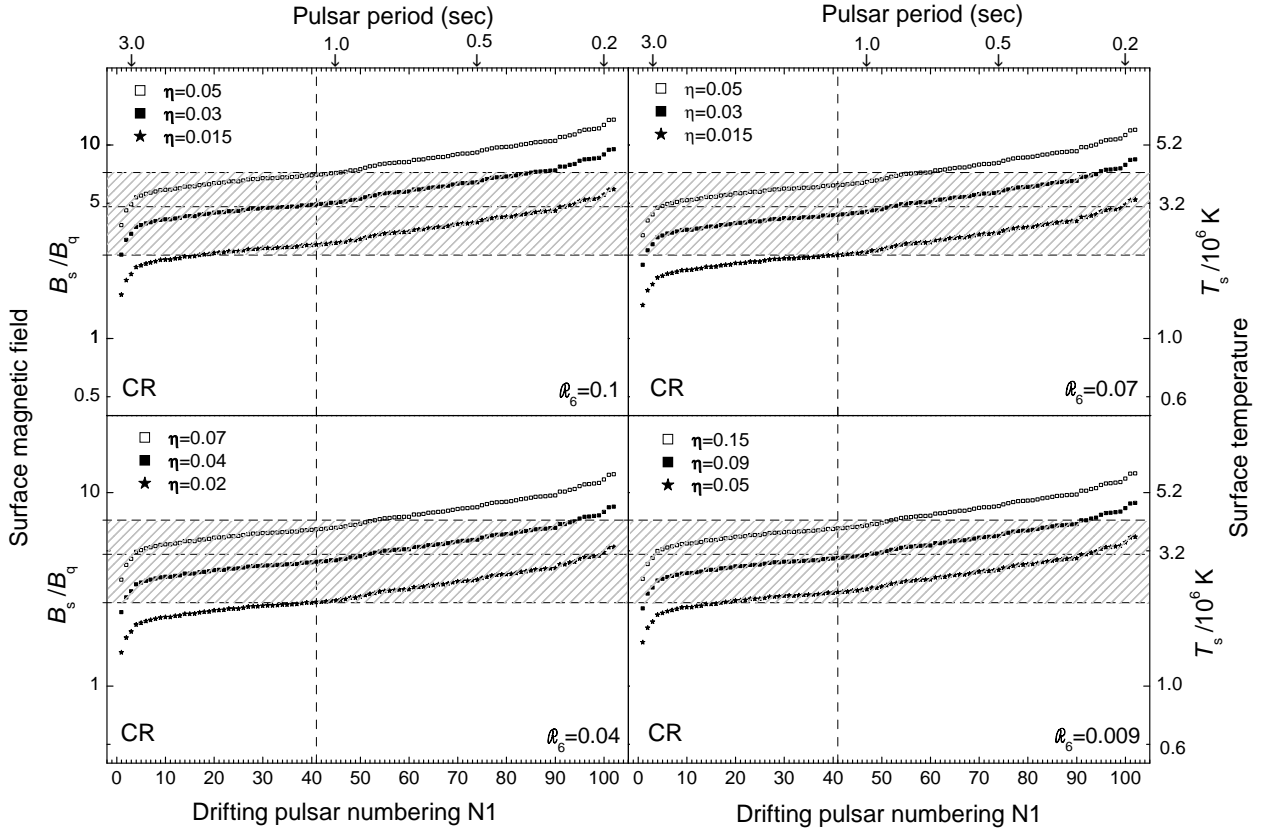


Fig. 1.— Models of partially screened inner acceleration regions (PSG) driven by curvature radiation seed photons above positively charged (ion case) polar cap for 102 pulsars from Table 1, sorted according to pulsar period. The horizontal axes correspond to the pulsar number N1 (bottom) or pulsar period (top). The vertical axes correspond to the surface magnetic field B_s/B_q (left-hand side), or surface temperature $T_s/10^6$ K (right-hand side). The calculations were made for conditions corresponding to very strong ($B_s > 5 \times 10^{12}$ G) and curved ($0.1 > \mathcal{R}_6 > 0.005$) surface magnetic field. The vertical lines correspond to the case of PSR B0943+10 (N1=41) and the hatched area encompassing three horizontal lines correspond to the range of surface magnetic field and temperature inferred for this pulsar from the XMM-Newton observation (ZSP05). These models allow to read off the physical conditions existing in the acceleration region above the polar cap of a particular pulsar in the form of parameters such as B_s , \mathcal{R}_6 and η .

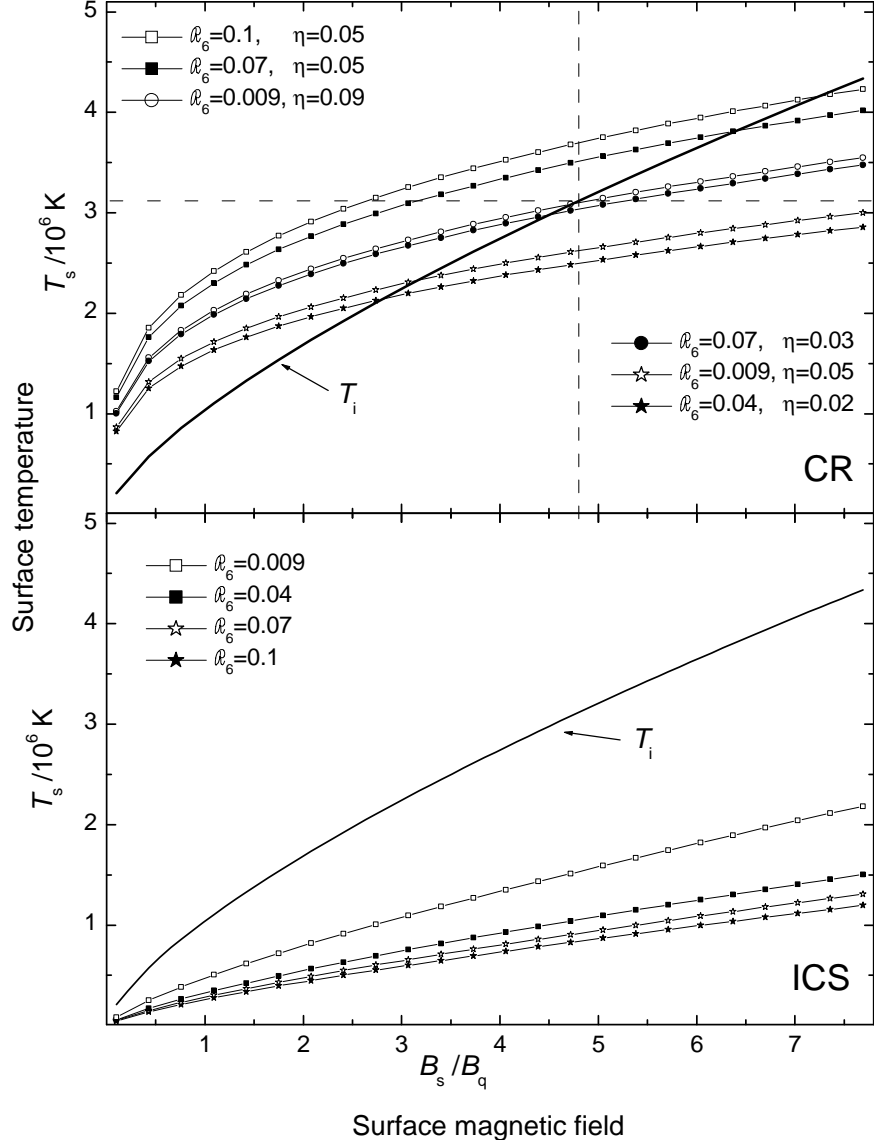


Fig. 2.— Dependence of the surface temperature on the surface magnetic field in the case of NTPSG for CR (upper panel) and ICS (lower panel) cases. Solid lines represent the critical ion temperature T_i , while the symbol-broken lines represent the actual surface temperature T_s for different combinations of the parameters \mathcal{R}_6 and η . As one can see only the CR case can work in pulsars with positively charged (ion case) polar cap. The solution for PSR B0943+10 marked by the dashed lines is $\mathcal{R}_6 = 0.009$, $\eta = 0.09$ and $T_s = 3.1 \text{ MK}$, implying $B_s = 4.8B_q \sim 2 \times 10^{14} \text{ G}$.

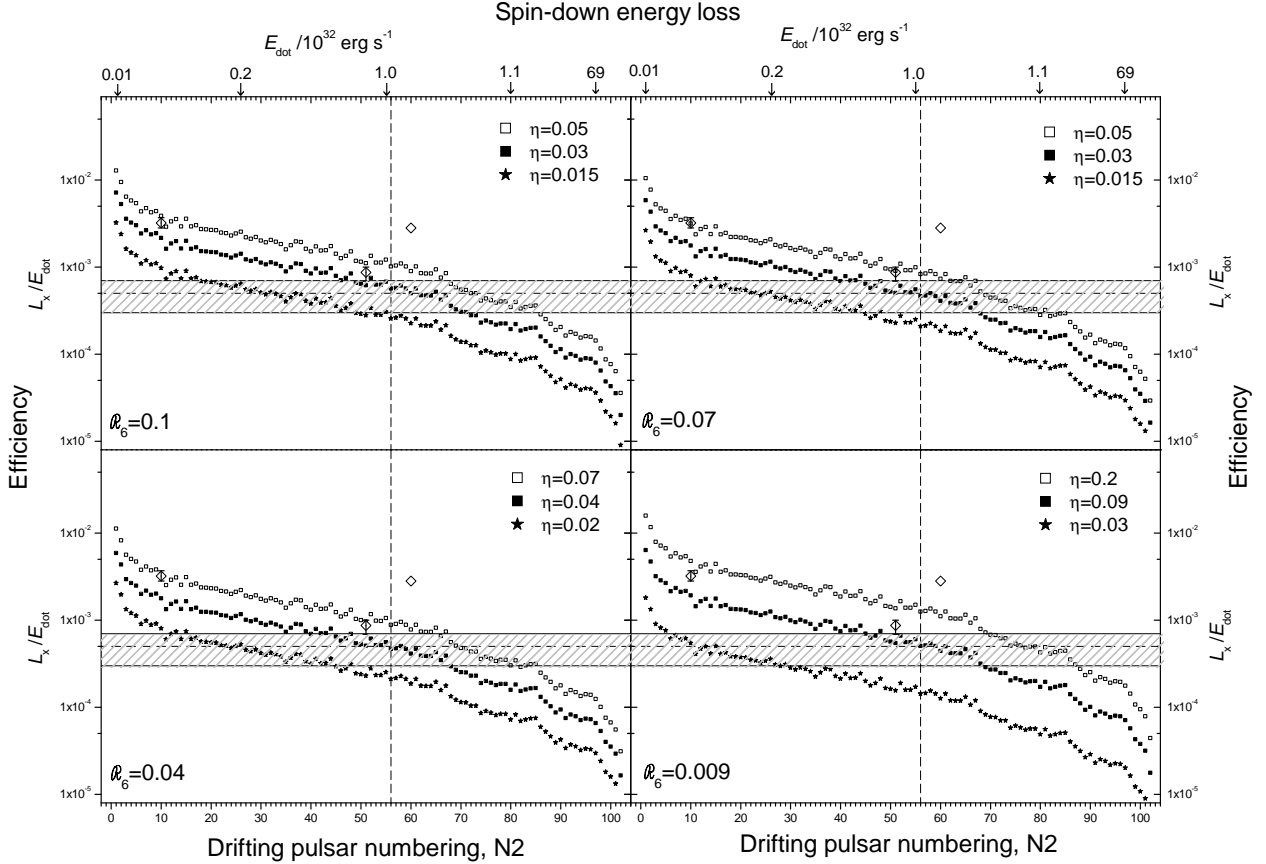


Fig. 3.— The thermal radiation efficiency from the hot polar cap for 102 pulsars from Table 1 for different parameters of the PSG marked in the legends. Pulsars are sorted according to the pulsar spin-down luminosity (N2 in Table 1). For clarity of presentation the surface field is fixed at $B_s/B_q=4.8$. The vertical dashed lines ($N2=56$) and three horizontal dashed lines ($L_x = 5 \pm 2 \times 10^{28}$ erg/s) within the hatched area correspond to the special case of PSR B0943+10 (Tables 1 and 2). Three other pulsars for which values of \dot{P}_3/P is directly determined from single pulse radio data are included as diamond symbols: B0826-34 ($N2=10$), B1133+16 ($N2=51$) and B0834+06 ($N2=60$).

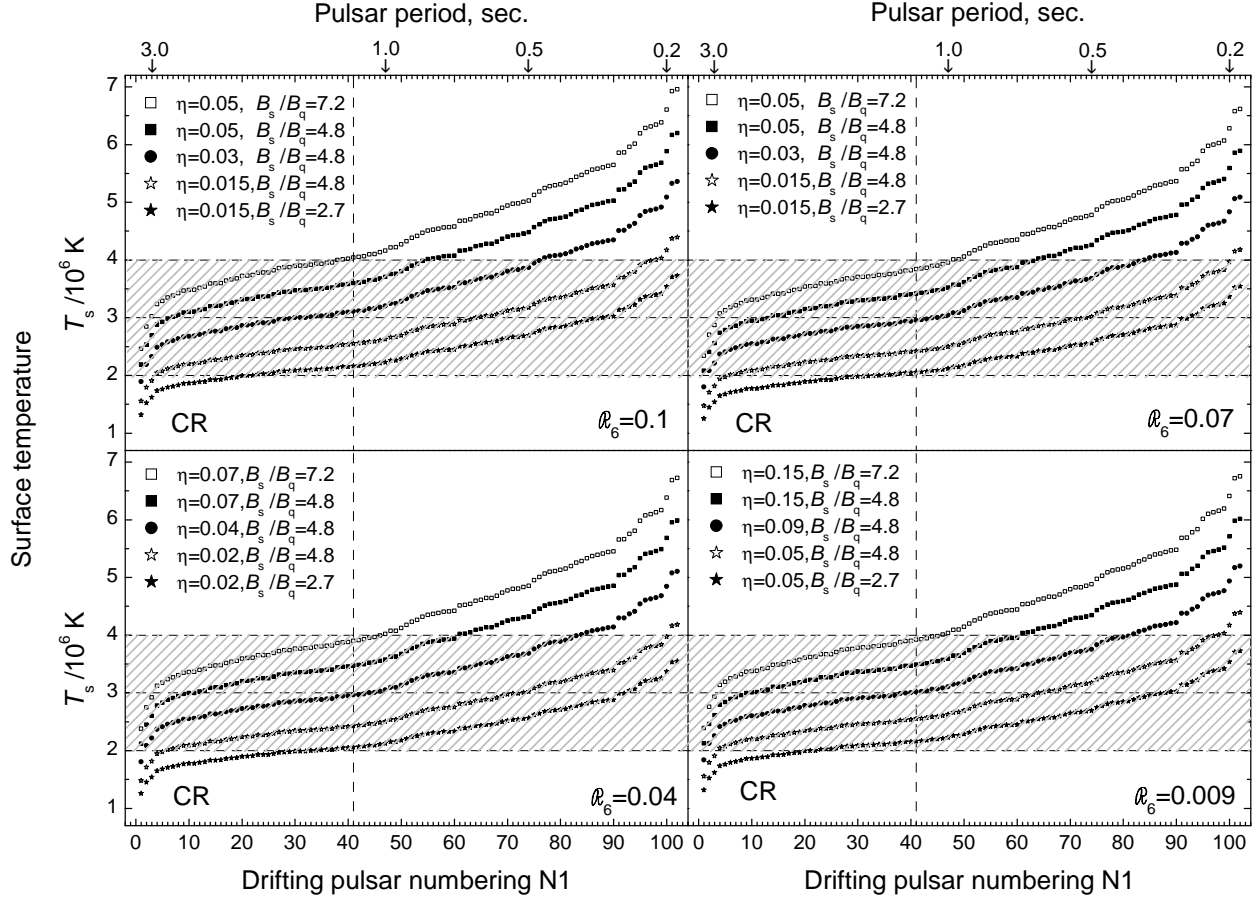


Fig. 4.— Surface temperature of hot polar cap for 102 pulsars from Table 1 for different parameters of the PSG marked in the legends. Pulsars are sorted according to the pulsar period (N1 in Table 1). The vertical dashed lines ($N_1=41$) and three horizontal dashed lines ($T_s = 3 \pm 1 \times 10^6$ K) within the hatched area correspond to the case of PSR B0943+10.

Table 1: Comparison of observed and predicted parameters

Name PSR B	\dot{P}_3/P		$L_x/\dot{E} \times 10^{-3}$		$L_x \times 10^{28}$		b $A_{\text{pc}}/A_{\text{bol}}$	$T_s^{(\text{obs})}$ 10^6 K	$T_s^{(\text{pred})}$ 10^6 K	B_d 10^{12} G	B_s 10^{14} G
	Obs.	Pred.	Obs.	Pred.	Obs.	Pred.					
0943 + 10	37.4	36	$0.49^{+0.06}_{-0.16}$	0.45	$5.1^{+0.6}_{-1.7}$	4.7	60^{+140}_{-48}	$3.1^{+0.9}_{-1.1}$	$3.3^{+1.2}_{-1.1}$	3.95	$2.37^{+0.53}_{-0.70}$
1133 + 16	(33^{+3}_{-3})	27^{+5}_{-2}	$0.77^{+0.13}_{-0.15}$	$0.58^{+0.12}_{-0.09}$	$6.8^{+1.1}_{-1.3}$	$5.1^{+1.0}_{-0.8}$	$11.1^{+46.6}_{-5.6}$	$2.8^{+1.2}_{-1.2}$	$2.1^{+0.5}_{-0.4}$	4.25	$0.47^{+0.71}_{-0.24}$
0826 - 34	14^{+1}_{-1}			$3.2^{+0.5}_{-0.4}$		$2.0^{+0.33}_{-0.25}$					2.74
0834 + 06	15			2.8		37					5.94
0809 + 74	150			0.003		0.009					0.5
0633 + 17		400	0.004		15		25	$1.9^{+0.3}_{-0.3}$	2.13	1.6	0.4

Table 2: List of 102 pulsars with drifting subpulses compiled from R86, GM02 and WES05. N1 and N2 refer to sorting according to pulsar period P and spin-down luminosity \dot{E} , respectively.

Name	N1	N2	Name	N1	N2	Name	N1	N2	Name	N1	N2
B0011+47	31	17	B0823+26	71	71	B1822-09	54	91	B1953+50	73	69
B0031-07	49	25	B0826-34	10	10	J1830-1135	1	11	B2000+40	50	53
B0037+56	40	50	B0834+06	28	60	B1839+56	15	18	J2007+0912	76	61
B0052+51	6	40	B0919+06	78	97	B1839-04	11	5	B2011+38	97	100
B0136+57	94	99	B0940+16	42	3	B1841-04	47	64	B2016+28	69	37
B0138+59	33	13	B0943+10	41	56	B1844-04	67	98	B2020+28	89	86
B0144+59	100	85	B1039-19	24	19	B1845-01	61	76	B2021+51	72	79
B0148-06	20	8	B1112+50	14	28	B1846-06	21	74	B2043-04	18	22
B0301+19	23	24	B1133+16	36	51	B1857-26	65	38	B2044+15	38	7
B0320+39	3	2	B1237+25	25	20	B1859+03	62	80	B2045-16	8	46
B0329+54	59	66	B1508+55	56	72	B1900+01	57	70	B2053+36	99	84
B0450+55	90	87	B1530+27	39	29	J1901-0906	12	16	B2106+44	81	44
B0523+11	87	48	B1540-06	60	54	B1911-04	52	68	B2110+27	35	47
B0525+21	2	35	B1541+09	55	41	B1914+13	93	96	B2111+46	46	32
B0540+23	95	101	B1604-00	80	65	J1916+0748	70	88	B2148+63	84	58
B0609+37	92	52	B1612+07	34	45	B1917+00	29	63	B2154+40	19	39
B0621-04	45	33	B1642-03	83	83	B1919+21	26	27	B2255+58	85	92
B0626+24	75	75	J1650-1654	13	30	B1923+04	43	49	B2303+30	17	34
B0628-28	30	62	B1702-19	91	95	B1924+16	68	89	B2310+42	88	55
B0727-18	74	94	B1717-29	64	59	B1929+10	98	90	B2319+60	5	31
B0740-28	101	102	B1737+13	53	57	B1933+16	86	93	B2324+60	96	81
B0751+32	22	21	B1738-08	7	14	B1937-26	82	73	B2327-20	16	42
B0809+74	27	4	B1753+52	4	6	B1942-00	44	23	J2346-0609	37	36
J0815+0939	63	26	B1804-08	102	67	B1944+17	77	15	B2351+61	48	77
B0818-13	32	43	B1818-04	66	82	B1946+35	58	78			
B0820+02	51	9	B1819-22	9	12	B1952+29	79	1			